



# Microstructural and other properties of copper slag–coal bottom ash incorporated concrete using fly ash as cement replacement

Gaurav Singh<sup>1</sup> · ShriRam<sup>1</sup>

Received: 4 October 2022 / Accepted: 11 January 2023 / Published online: 23 January 2023  
© Springer Nature Switzerland AG 2023

## Abstract

Increased demand for concrete leads to an increase in utilization of cement and sand, and increased consumption of cement leads to increased CO<sub>2</sub> emissions. Furthermore, mining restrictions in certain areas and the growing need for natural ecological sustainability lead to additional problems with river sand availability. This study promotes the utilization of industrial waste in concrete for long-term environmental sustainability and safe disposal. Out of various types of industrial byproducts, combined use of copper slag and bottom ash as sand and simultaneously fly ash as cement, the replacement has not yet been studied out. Hence, the primary goal of this research was to evaluate their usage in concrete to replace sand with copper slag and coal bottom ash waste, as well as cement with fly ash. Concrete mixtures were made using varying amounts of waste copper slag (CS) and bottom ash (CBA) (0–60%) in equal proportions as a partial substitute for natural sand, as well as fly ash (0–30%) as cement. Slump, unit weight, split tensile strength, compressive strength, and microstructural characteristics such as X-ray diffraction, SEM, and EDS of concrete mixtures were investigated. Test results reveal that workability, compressive and split tensile strength improve with increment in percentage replacement of FA, CS, and CBA. Improvement in strength with the percentage replacement is also confirmed by change in morphology by SEM and X-ray diffraction analyses.

**Keywords** Fly ash · Waste copper slag · Bottom ash · Characterization of materials · X-ray diffraction · SEM and EDS · Unit weight · Slump · Compressive strength · Split tensile strength

## Introduction

Concrete is the most often utilized material in the building and construction industry [1]. The Indian construction industry uses approximately 400 million tonnes (mt) of concrete per year, with a projected growth of 1000 million tonnes in less than a decade [2]. By 2050, the demand for concrete is expected to rise to over 7.5 billion m<sup>3</sup> approximately 18 billion tonnes (bt) each year [3]. Increased demand for concrete leads to increased use of cement and sand, and increased consumption of cement leads to increased CO<sub>2</sub> emissions, which can be reduced by substituting additives for cement [4]. The cement manufacturing process emits greenhouse

gases, which cause global warming. The cement industry has long been among the most carbon dioxide emitters. Cement plants account for almost 8% of all anthropogenic carbon dioxide emissions worldwide [5]. With more than 7% of global installed capacity, India is the world's second-largest cement maker. Because of increased demand in sectors such as housing, urban planning, and commercial establishment, India's cement manufacturing capacity is expected to increase to 550 million tonnes per year by 2025 [6]. The coarse and fine aggregates account for at least half of the overall volume of concrete. Natural resources, such as sand, are clearly running out [7]. Mining restrictions in particular locations, as well as the rising requirement for natural ecological sustainability, exacerbate the availability of sand. Finding novel recycled material for ecological development in order to drastically minimize natural resource use has become vital in order to preserve future generations' interests. Increased use of environmental assets resulted in increased industrial debris and environmental degradation [8]. These circumstances have compelled scholars to devise solutions that would lead to much-needed sustainable

---

✉ Gaurav Singh  
gsbiya90@gmail.com  
ShriRam  
src\_gkp@rediffmail.com

<sup>1</sup> Department of Civil Engineering, Madan Mohan Malaviya University of Technology, Gorakhpur, Uttar Pradesh 273010, India

development. In place of cement and sand, the utilization of industrial wastes such as waste glass, rubber tire trash, foundry sand, slag, coal ash, and marble powder can contribute to sustainable development [9]. Rapid industrialization and urbanization result in a considerable amount of toxic industrial waste that endangers human health and the environment. As the amount of industrial trash grows each year, one of the primary issues is a lack of land for safe disposal. As a result, safe waste disposal is critical for maintaining a sustainable ecosystem.

When coal is burned in a coal-ignited boiler, it produces ash, some of which is retrieved from the lower surface of the furnace and referred to as coal bottom ash (CBA), some of which is transported upward through the furnace's warm combustion gases and retrieved by collecting devices as fly ash (FA). For many years, coal-fired thermal power stations have produced massive amounts (20–80%, respectively) of CBA and fly ash. FA and CBA are wastes of the combustion of pulverized coal. When used jointly, they maximize the usage of disposal waste, which has the potential to lessen environmental effects [3]. Bottom ash chemical and physical characteristics can differ depending on the origin, type, as well as tenuity of the source fuel, along with power station process variables [10]. The world's total energy output from coal-ignited power stations is somewhere around 38% [11], with India accounting for more than 65% [12]. A lot of work is being done in developing countries like India in the field of thermal power generation, which results in the generation of coal ash. India's power generation is approximately 75% thermal (coal, gas, and oil-based), with approximately 70% being coal-based. Thermal power plants currently generate approximately 197 million tonnes of coal ash per year, and by 2032, approximately 600 million tonnes of ash would be produced. In 2020–21, India's coal plants produced 232.56 million tonnes of fly ash [13]. A sufficient amount of fly ash is currently available, and its availability is expected to remain fairly consistent over the next few decades. CBA is grainy, vitreous, coarse, and porous, and ranges in color from gray to blackish [14, 15]. It is predominantly composed of silica oxides, iron oxides, and alumina oxides, in addition to other minerals such as magnesium, calcium, and sulfate [3].

To fulfill the requirements of the construction sector, 48.3 bt of construction aggregate was generated worldwide annually [16]. While global copper output surpassed 20.6 mt, Chile was the largest manufacturer at the time, with 5.7 mt [17]. China generated more than half of total worldwide copper slag manufacture in the same year, while India produced approximately 3.5 percent of overall production, with 2.4 mt produced, and other nations such as Chile, Russia, and Japan contributed 8, 3.5, and 9%, respectively [18]. Copper slag is a byproduct of metallic copper extinction and smelting. Copper liquid sinks throughout the smelting process due to

its high density; on the other hand, it remains segregated on the top for further extraction and cooling. It mostly constitutes silica oxide ( $\text{SiO}_2$ ) with iron oxides ( $\text{Fe}_2\text{O}_3$ ). However, it also incorporates oxides of alumina, magnesium oxide ( $\text{MgO}$ ), and calcium oxide ( $\text{CaO}$ ) [19–21]. It also includes a certain quantity of metals that are heavy; however, according to leaching studies conducted under active conditions; these amounts are lower than the toxicity limit [22]. South Korean, Japanese, and Indian standards all approve copper slag as an aggregate. The building and construction authorities in Singapore also provide rules that copper slag is being used as a renewable and sustainable material. According to data, when one tonne of copper is produced, approximately 2.3–3 tonnes of copper slag is produced, and copper slag output is predicted to reach 55 metric tonnes or perhaps more in the year so [23].

Numerous research works have been conducted on the combined use of industrial waste such as waste foundry sand and coal bottom ash [11], fly ash, blast furnace slag and coal bottom ash [10, 24], non-ground blast furnace slag and coal bottom ash [25], and few studies have been conducted on the combined use of copper slag and coal bottom ash in concrete [26] and in geopolymer mortar [27] to the author's knowledge yet. There are very few research studies conducted yet on concrete containing copper slag and coal bottom ash. Hence, this research work focuses on the practical percentages of fly ash (FA), copper slag (CS), and coal bottom ash (CBA) in concrete. The mechanical (compressive strength and split tensile strength), physical, and microstructural characteristics (XRD, SEM, and EDS) of concrete incorporating FA, CS, and CBA are investigated in this research study. Microstructural test findings are also compared to destructive test results. The current research investigates the physical, mechanical, and microstructural characteristics of concrete containing fly ash as a substitute for cement up to 30% with a 5% interval and CS and CBA as a replacement for natural sand in an equal percentage ranging from 0 to 60% with an equal interval of 10%.

## Materials

Fly ash is collected from a nearby thermal power station. The entire sum of the ingredients  $\text{SiO}_2$ ,  $\text{Al}_2\text{O}_3$ , and  $\text{Fe}_2\text{O}_3$  was found to be larger than 70%, confirming the class F fly ash standards in accordance with BIS 3812 (part 1)-2003. The physical characteristics and elemental composition of fly ash are demonstrated in Tables 1 and 2, respectively. The SEM (scanning electron microscopy) morphology reveals that the fly ash is spherical and regular in shape (Fig. 1), and the EDS (energy-dispersive spectroscopy) and XRD (X-ray diffraction) analysis revealed that the fly ash is largely made of silica, alumina, and iron (Figs. 2 and 3, respectively).

**Table 1** Physical characteristics of fly ash

Property	Fly ash	BIS value
Fineness (m <sup>2</sup> /kg)	423	> 320
Lime reactivity, N/mm <sup>2</sup>	5.5	> 4.5
Compressive strength (N/mm <sup>2</sup> )		
28 days	40.5	–
Soundness by autoclave (%)	0.16	< 0.8
Particles retained on 45-micron IS sieve wet sieving in, %	24.3	< 34

Portland Pozzolana Cement of 53.1 N/mm<sup>2</sup> conforming to IS 1489–2015 (Part 1) [28] with consistency as 30%, initial setting time as 160 (min), final setting time as 250 (min), Le-chat expansion as 1 (mm), autoclave expansion as 0.180 (%), specific gravity (SG) as 3.52 and fineness as 340 (m<sup>2</sup>/kg), was used. The river sand from Banda, Uttar Pradesh, was utilized and conformed to BIS 383 (2016) [29]. Table 3 depicts the physical characteristics of the sand, copper slag, and coal bottom ash utilized in this study. The crushing value, impact value, abrasion value, specific gravity, and water absorption of coarse aggregate in 10 and 20 mm sizes are illustrated in Table 4. The particle size distribution of sand, copper slag, coal bottom ash, and coarse aggregate is shown in Table 5. The coal bottom ash came from a nearby thermal power plant. Bottom ash was graded in accordance

with BIS 383–2016, just like river sand. Copper slag was granular in shape, with angular sharp edges and a multi-faceted appearance. Birla Copper slag was used in this investigation. In this study, copper slag with a SG of 3.51 was used.

### Concrete mixtures and specimens preparation

Seven mixtures were prepared, one of which was the reference mix (FM0), and the others were fly ash-based mixes named FM5, FM10, FM15, FM20, FM25, and FM30, and tests were conducted on both freshly mixed and hardened mixed concrete at various curing time. Cement, water, and coarse aggregate (CA) concentrations were held constant at 350, 175, and 1268 kg/m<sup>3</sup>, respectively. For each mixture except for the reference mix, the amount of natural sand by mass was equally replaced with CS and CBA varied from 0 to 60% at a rate of 5% increment, i.e., (5% CS + 5% CBA), and simultaneously cement was replaced with FA. The percentage of fly ash ranged from 0 to 30% by mass with an increment of 5%. A concrete mixer with a capacity of 0.02 m<sup>3</sup> was used. To begin, all ingredients were weighed using a weighing balance. Weighed amounts of cement, fly ash, sand, coal bottom ash, and copper slag were dry mixed for one minute to achieve uniform color with no clusters of cement, sand, fly ash, and copper slag.

**Table 2** Chemical composition of fly ash and cement

Materials	SiO <sub>2</sub> + Al <sub>2</sub> O <sub>3</sub> + Fe <sub>2</sub> O <sub>3</sub>	MgO	SO <sub>3</sub>	Na <sub>2</sub> O	Cl	LOI
Fly ash	90.12	1.83	0.86	0.39	0.021	2.08
Cement	–	4.48	1.70	–	0.005	1.09

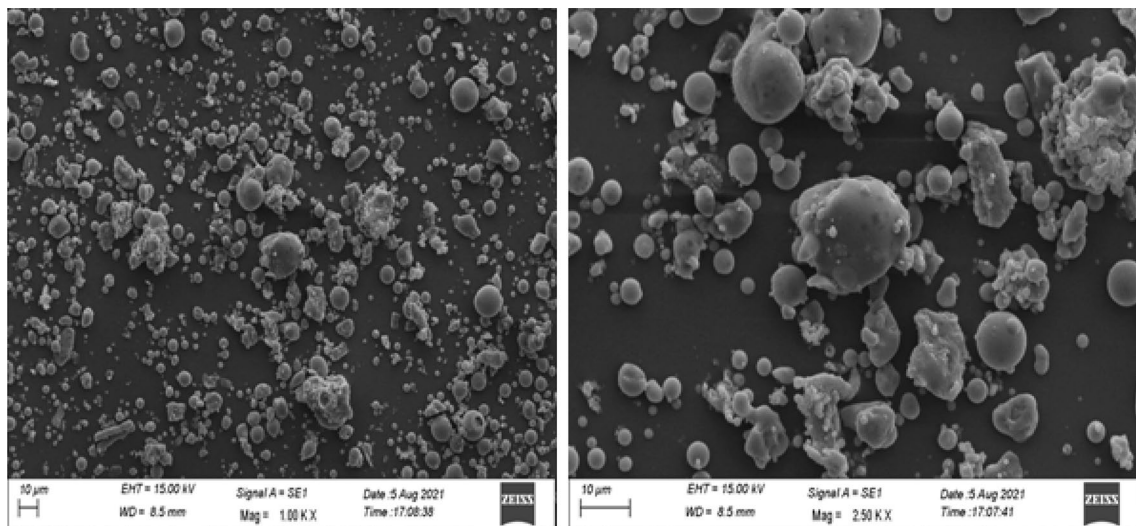


**Fig. 1** SEM morphology of fly ash

Fig. 2 EDS spectrum of fly ash

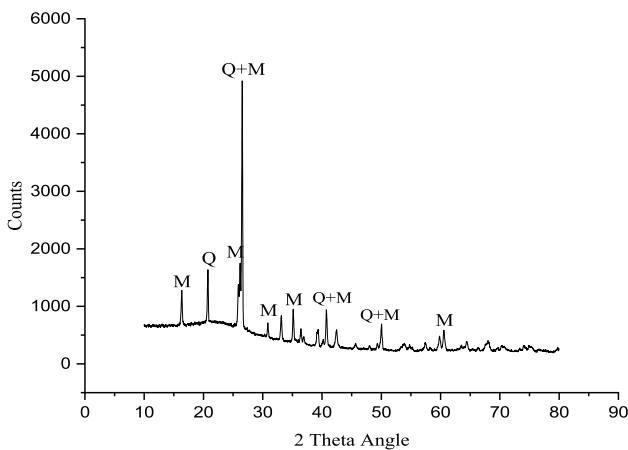
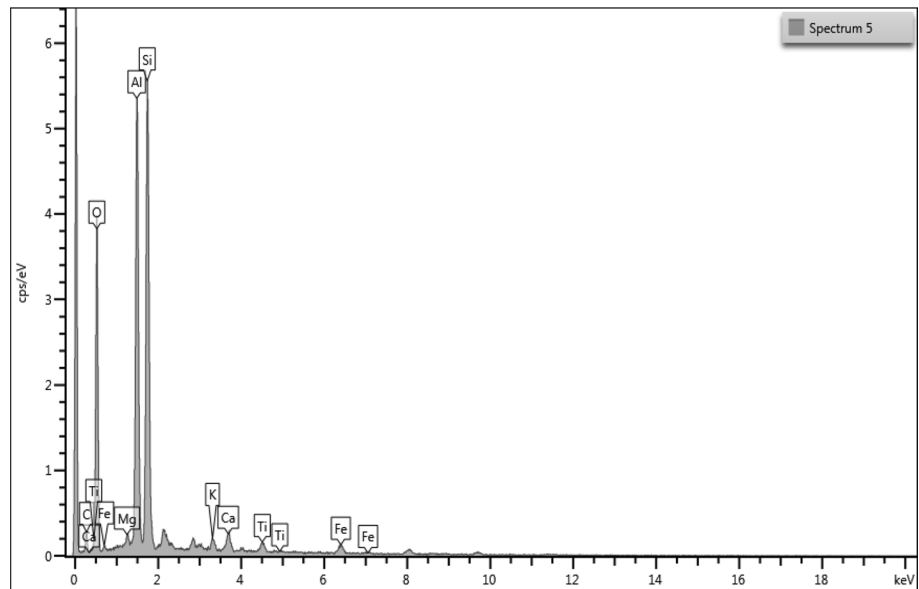


Fig. 3 X-ray diffractogram of fly ash (*M* mullite, *Q* quartz)

Table 3 Physical properties of fine aggregate

Properties	Natural sand	Copper slag	Coal bottom ash
Bulk density, kg/m <sup>3</sup>	1683	1870	1210
Fineness modulus	3.11	3.41	—
Water absorption, %	0.81	0.36	4.18
Specific gravity	2.58	3.51	2.11

Table 4 Physical properties of coarse aggregate

Aggregate size (mm)	Crushing value (%)	Impact value (%)	Abrasion value (%)	Specific gravity	Water absorption (%)
10	22.09	9.23	15.60	2.72	1.42
20	24.02	8.31	17.72	2.73	1.21

Coarse aggregate was then incorporated in a weighed amount and dry blended for 1 min to achieve a homogeneous mix. The addition of aggregate after mixing the binder can help to reduce the amount of water used in the process and is also advantageous for large-scale production because it results in a 10–20% increase in strength [30]. A specified amount of water was divided into 2 equal portions. The first half portion of the water was added to the dry mix of concrete, and after uniform mixing of water, the remaining portion of water was added to the wet mix. Adding water in two steps avoids cluster formation or honeycombing of concrete mixes. The schematic procedure of the casting process with allotted time at each mixing stage is illustrated in Fig. 4. Before casting the specimens, all of the molds were lubricated. Each concrete mixture's compressive strength was determined by casting a cube size of 150 mm × 150 mm × 150 mm. For measuring the splitting tensile strength of concrete mixtures, cylinders of size 150 mm × 300 mm were cast. After 24 ± 1 h of adding water to the concrete mixture, the specimens were demolded. After demolding, the cube and cylinder specimens were cured in water at room temperature. The final mix proportion was determined after several experiments, as indicated in Table 6.

**Table 5** Particle size distribution of the coal bottom ash, copper slag, sand and coarse aggregate used in this research study

Sieve sizes (mm)	% Passing			
	CBA	CS	Sand	Coarse agg
40	–	–	–	100
20	–	–	–	98.47
10	100	100	100	35.7
4.75	99.7	98.85	94.5	0.9
2.36	99.1	93.65	78.5	–
1.18	93.9	49.25	56	–
0.6	55.2	15.75	41.3	–
0.3	1.6	0.9	14.2	–
0.15	0	0	4.6	–

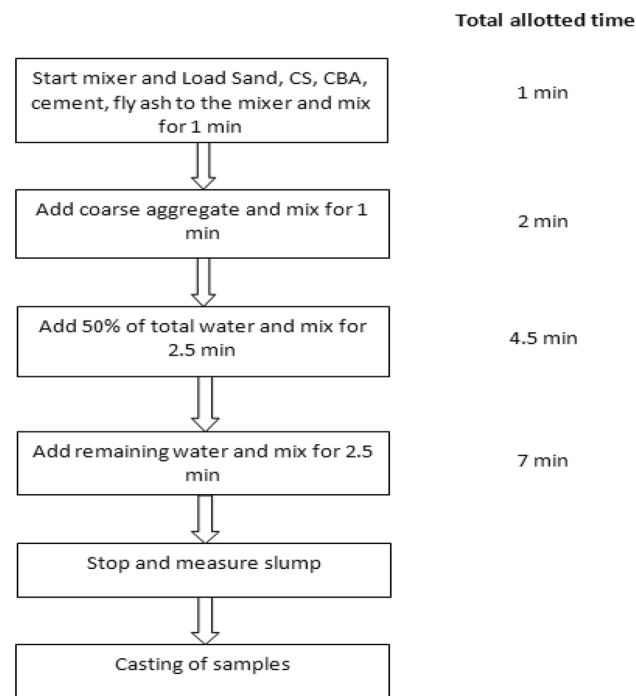


**Fig. 4** Schematic procedure of the casting process with allotted time at each mixing stage

### Experimental procedure

A slump test was performed to determine the workability of the concrete mixture in accordance with BIS 1199–1959. To find the unit weight of prepared concrete mixtures, cubic specimens were taken, did weigh over 28 days, and each specimen was kept at ambient temperature [12]. Concrete strength tests were conducted on concrete cubes of 7, 28, and 91 curing days using a compression testing machine with a load-carrying range of 2000

**Table 6** Proportioning of all concrete mixtures

Concrete mixtures	Description	Fly ash (%)	Cement (kg)	Fly ash (kg)	Crushed stone (kg)	Sand (kg)	Copper slag (kg <sup>3</sup> )	CBA (kg)	w/c	Water (lt)
FM0	Reference	0	350	0	1268	597	0	0	0.50	175
FM5	5% CS + 5% CBA	5	332	18	1268	537.3	29.85	29.85	0.50	175
FM10	10% CS + 10% CBA	10	315	35	1268	477.6	59.7	59.7	0.50	175
FM15	15% CS + 15% CBA	15	297	53	1268	417.9	89.55	89.55	0.50	175
FM20	20% CS + 20% CBA	20	280	70	1268	358.2	119.4	119.4	0.50	175
FM25	25% CS + 25% CBA	25	262	88	1268	298.5	149.25	149.25	0.50	175
FM30	30% CS + 30% CBA	30	245	105	1268	238.8	179.1	179.1	0.50	175



**Fig. 5** Compressive strength test on cube sample



KN and a standard loading rate in compliance with IS 516 [31]. Figure 5 shows the compressive strength test setup with a cube mounted. The splitting tensile strength of concrete test samples was determined after 28 days of curing according to IS 5816 [32]. SEM images were captured using fractured segments from the core of reference and fly ash-based concrete mixtures cube samples retrieved from the compressive strength test for SEM morphology and EDS analysis. For this analysis, concrete fracture segments were placed on the SEM stub, and pictures were caught in backscattered electrons imaging mode. Scanning electron micrographs of concrete samples were obtained after 28 days of curing. The concrete samples were covered with a thin layer of gold before being placed on the SEM stem, making them electrically conductive. The cement pastes were sieved through a 90-micron sieve after being removed from the concrete samples engendered by the compressive strength test on cubic samples after curing for 28 days for XRD analysis. The XRD experiment was performed in 2 theta angle of 0.017 degree steps for a diffraction angle of 2 theta in range of 10 degree to 80 degree. The XRD (X-ray diffraction) patterns and relative peak intensity have been determined. The data are analyzed using freeware Match 3 software. Experimental setups for SEM, EDS, and XRD analysis were the same as Singh et al. [26].

## Discussion of results

### Slump and unit weight

The workability of concrete mixtures was determined by slump test as per BIS 1199. The slump value for all concrete mixtures is shown in Fig. 6. Results show that workability gradually improved with the increase in replacement

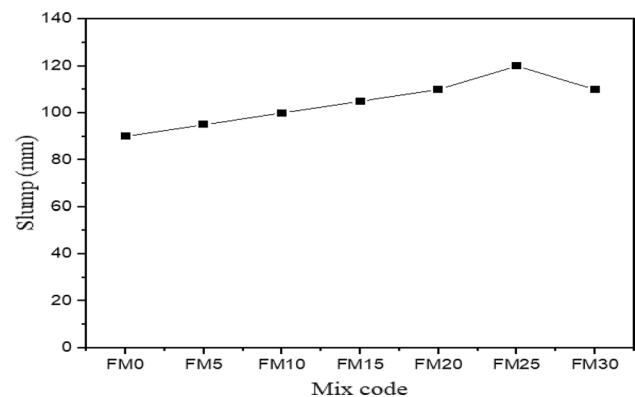


**Fig. 6** Slump value of concrete mixtures



**Fig. 7** Slump value of reference mix

of cement by fly ash percentage varied from 0 to 30%. The slump value for the Reference concrete mix (FM0) was found to be 90 mm shown in Fig. 7. It is increased up to 25% cement replacement by fly ash due to the spherical shape of fly ash particles; after that, it decreases. The workability of CS-CBA-incorporated concrete mix improves with the percentage increment of fly ash due to the spherical shape of fly ash particles confirmed by SEM image. The spherical form of fly ash particles minimizes friction between cement and aggregates, resulting in increased slump value of concrete mixtures. Similar findings were reported by other researchers [33, 34]. In the FM30 mix, slump value was found lower than the preceding one it is because of the higher quantity of coal bottom ash which possesses higher water absorption and absorbed some water internally due to its porous nature.

As the replacement percentage of (CS + CBA) increases, the unit weight of concrete mixtures decreases [26]. 28 days unit weight of fly ash-based concrete mixtures at 5, 10, 15, 20, 25, and 30% were 2457.83, 2461.52, 2455.93, 2469.25, 2488.16 and 2410.1 kg/m<sup>3</sup>, respectively, whereas for reference or control mix it is 2476 kg/m<sup>3</sup>. The use of fly ash caused a minor difference in unit weight due to the specific gravity of fly ash which is lesser than cement.

### Compressive strength and split tensile strength

Seven-, 28-, and 91-day compressive strength test results of reference mix and fly ash-based mixes containing CS and CBA as natural sand with fly ash as cement replacement varies from 0 to 30% are presented in Fig. 8. The compressive strength of reference concrete after 7 days of curing was 51.84% of

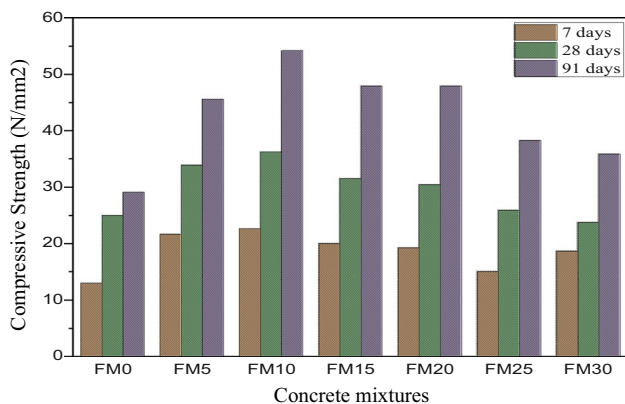


Fig. 8 Seven-, 28-, and 91-day compressive strength of concrete mixtures

its strength after 28 days of curing. The gained strength of fly ash-based concrete mixtures at 28 days was 63.89, 62.43, 63.58, 63.21, 57.98, and 46.97% for 5, 10, 15, 20, 25, and 30% cement replacement with fly ash, respectively. The strength of fly ash-based mixtures FM5, FM10, FM15, FM20, FM25, and FM30 after 28 days of curing was 33.87, 36.27, 31.49, 30.4, 25.92, and 23.77 N/mm<sup>2</sup>, respectively, especially in contrast to 25 N/mm<sup>2</sup> of reference mix. Because of the higher density packing, the FM10 concrete mix has a higher compressive strength.

When the CS and CBA concentrations were increased to a certain limit, the 28-day compressive strength of the concrete mixtures improved [26]. In addition, using fly ash as a partial cement replacement increased compressive strength. A thorough look at the strength gain between 28 and 91 days demonstrates that the concrete mixes containing fly ash attained more strength during this time period. The compressive strength of concrete mixtures prepared with 5, 10, 15, 20, 25, and 30% fly ash increased by 34.7, 49.5, 52.40, 57.81, 49.8, and 50.9% from 28 to 91 days, respectively, whereas the reference mix increased by 16.5%. The significantly greater strength gain for fly ash-prepared mixes was believed to be due to the pozzolanic impacts of fly ash in their later years [35].

The findings indicate that as the fly ash concentration grew, so did the split tensile strength of the prepared mixes. After 28 days of curing, the splitting tensile strength of all fly ash-based (FA + CS + CBA) concrete mixes was approximately 7–9% of their compressive strength, whereas the split tensile strength of the reference mix was 5.89% of its compressive strength. Table 7 depicts splitting tensile–compressive strength ratios that are consistent with previous research [12].

### Microstructural analysis

#### SEM and EDS

SEM equipment [Carl Zeiss Evo 50 Germany] was used for the microstructure study. After 28 days, each mixed sample was scanned under electron microscopy to acquire SEM images (Micrographs). Throughout the test, secondary electron images were captured. The microstructural formations of concrete mixtures have a significant impact on their strength and physicochemical characteristics. Electron microscopy analysis is used to investigate the morphology of concrete mixtures. Concrete's surface morphology is heterogeneous and difficult to comprehend. Calcium silica hydrate serves as the most crucial stage of the cementitious matrix, and numerous factors impact the mechanical performance of CSH phases such as the size of

Table 7 Split tensile–compressive strength ratios of concrete mixtures

Concrete mixture	FM0	FM5	FM10	FM15	FM20	FM25	FM30
Ratios (%)	5.89	7.09	8.13	8.92	9.21	9.34	9.28



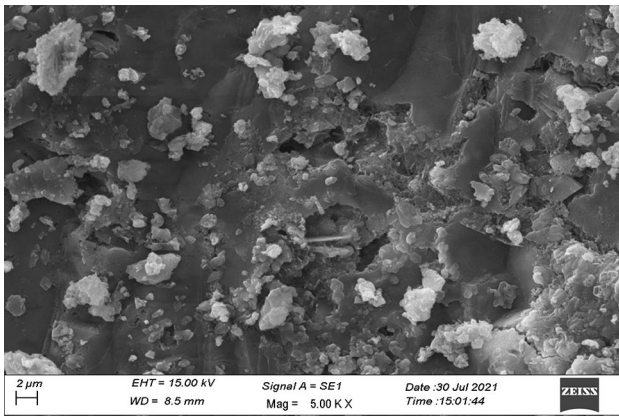


**Fig. 9** Secondary electron image of Reference mix (FM0)

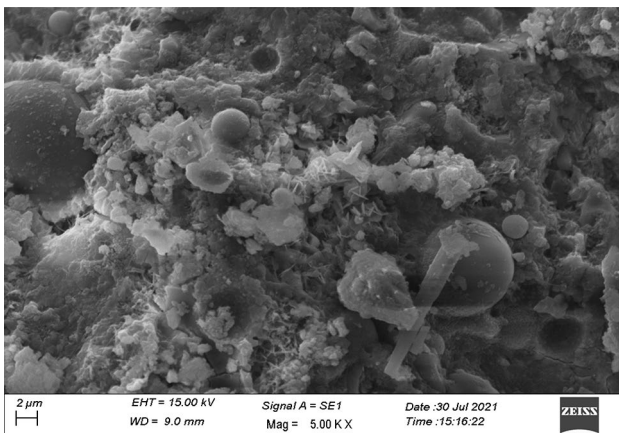


**Fig. 10** Secondary electron image of FM10 prepared mix

particles, form, dispersion and concentration, elemental composition, and particle alignment in the matrix [36]. Surface morphology through SEM pictures of reference mix and fly ash-based concrete mixtures containing 10, 15, and 30% fly ash as cement replacement is illustrated in Figs. 9, 10, 11, and 12. According to the previous studies [3], it is hypothesized that spherical and regular shape granules represent fly ash particles, which is confirmed by SEM analysis, and slightly dark matter/crystals in pictures show calcium silicate hydrate gel, and needle-long whisker morphology represents ettringite crystals. The SEM micrograph of the reference concrete mixture (FM0) at 5KX is shown in Fig. 9. The C–S–H gel has a slightly dark and fibrous gel formation visible in the image. Dense C–S–H gel and very few ettringite needles were seen in the FM10 concrete mix leading to strength increment. It is clearly visible that the utilization of (CS + CBA) as natural sand with fly ash as cement indicates enhancement of concrete strength which is significant as compared to the reference mix. In the case of the FM15 concrete mix, C–S–H gel, microcracks, and some fibrous structure was observed when 15% fly

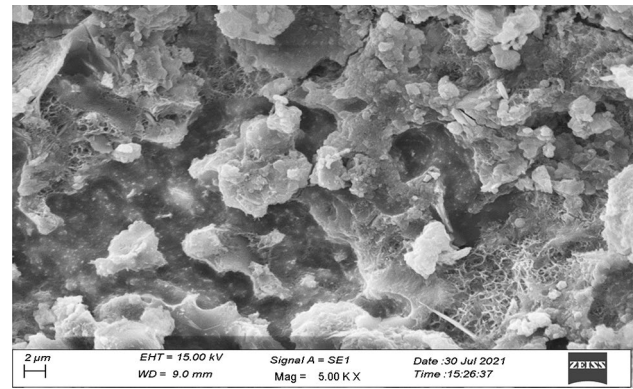
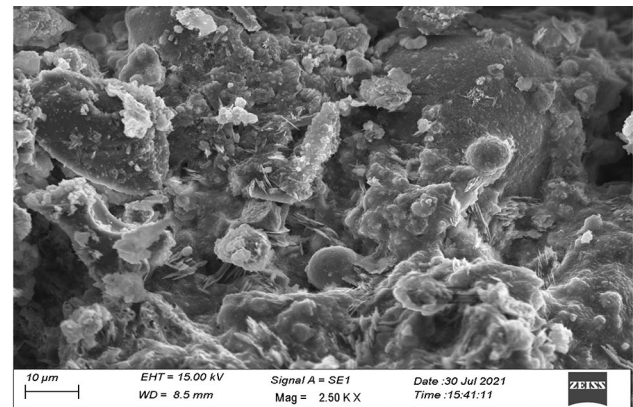
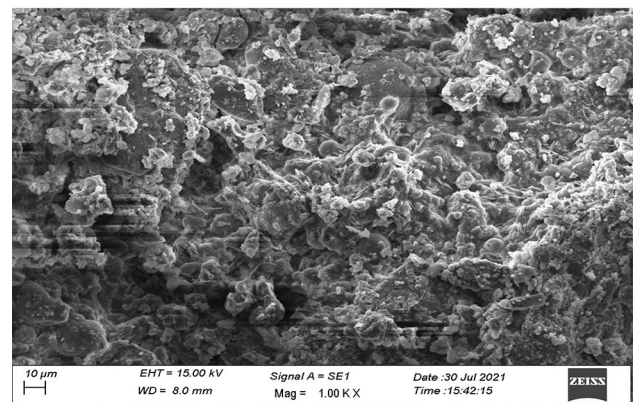


**Fig. 11** Secondary electron image of FM15 prepared mix



(a)



(b)

**Fig. 12 a** Secondary electron image of FM30 prepared mix. **b** Secondary electron image of FM30 prepared mix

ash is utilized, resulting in a decrease in strength compared to the previous one (FM10 mix). Figure 12a and b shows the SEM image of FM30 concrete mix at 2500X magnification and 1000X, respectively. The higher percentage of fly ash and CBA leads to a large number of voids and loosely packed structures in the FM30 concrete mix, resulting in a decrease in compressive strength.



Figures 13, 14, 15, and 16 show the results of EDS analysis on reference mix (FM0) and fly ash-based concrete

mixtures (FM10, FM15, FM30) containing 10, 15, and 30% fly ash as cement replacement. EDS analysis of the concrete

**Fig. 13** EDS spectra of reference mix (FM0)

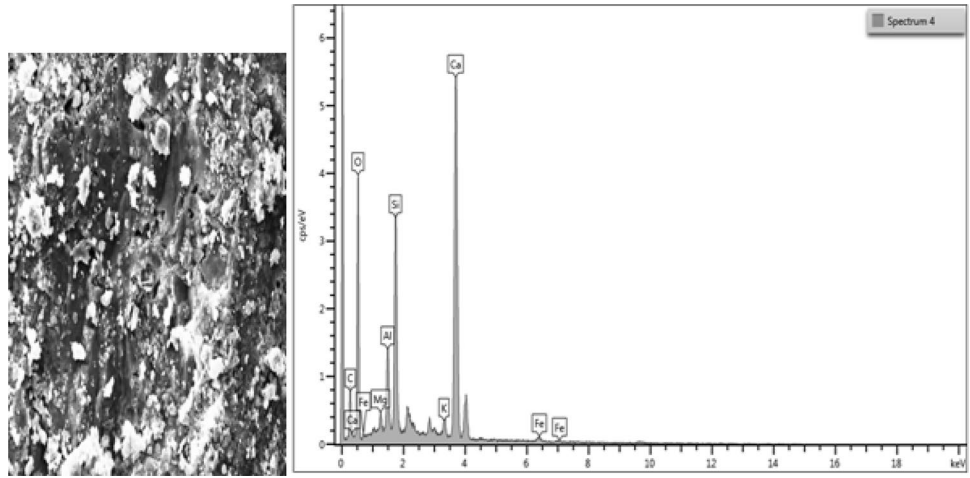


**Fig. 14** EDS spectra of FM10 prepared mix

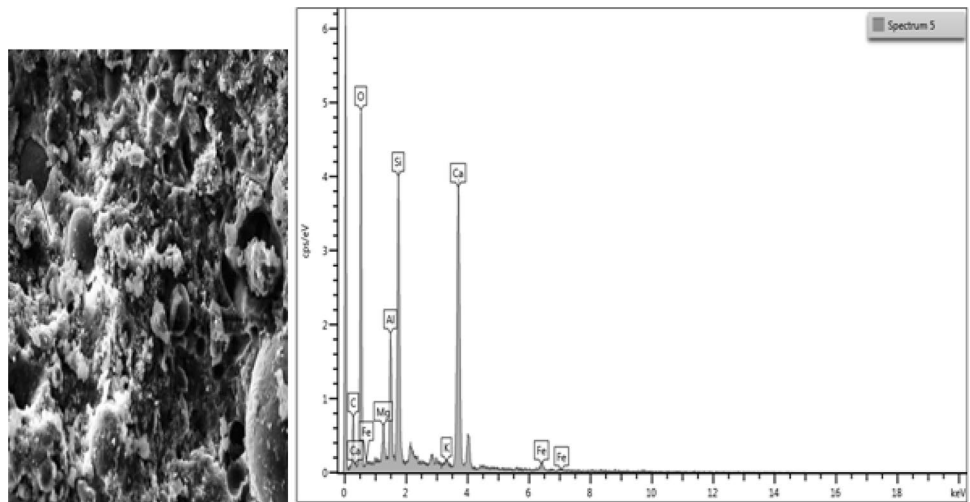


**Fig. 15** EDS spectra of FM15 prepared mix

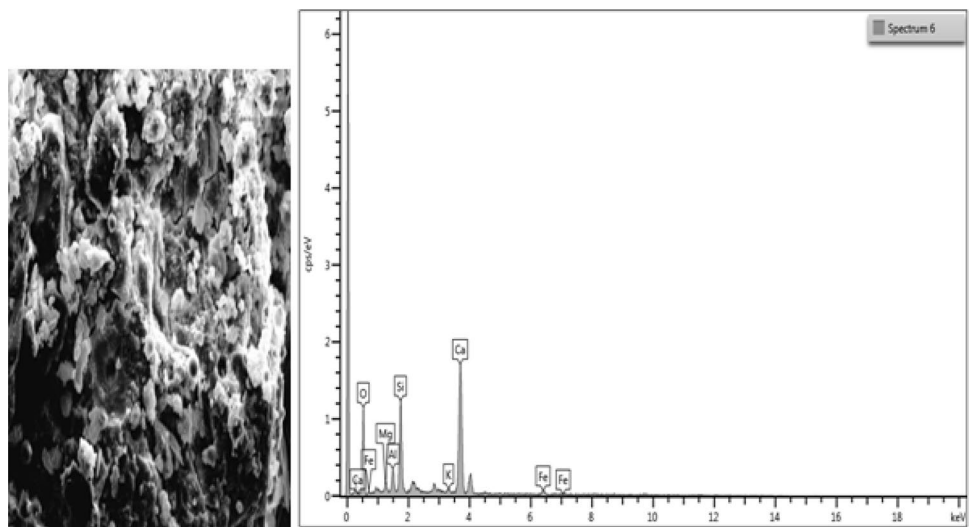


**Fig. 16** EDS spectra of FM30 prepared mix

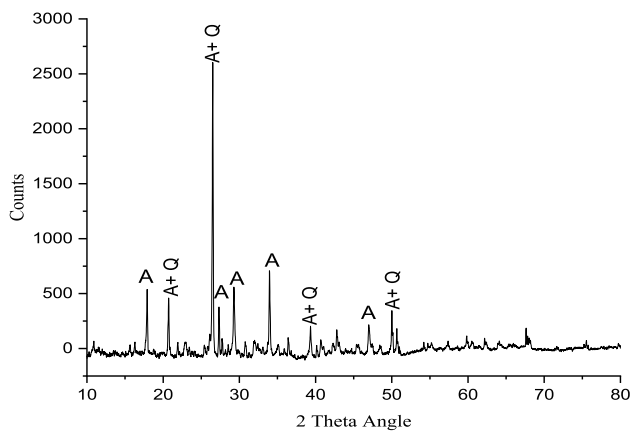
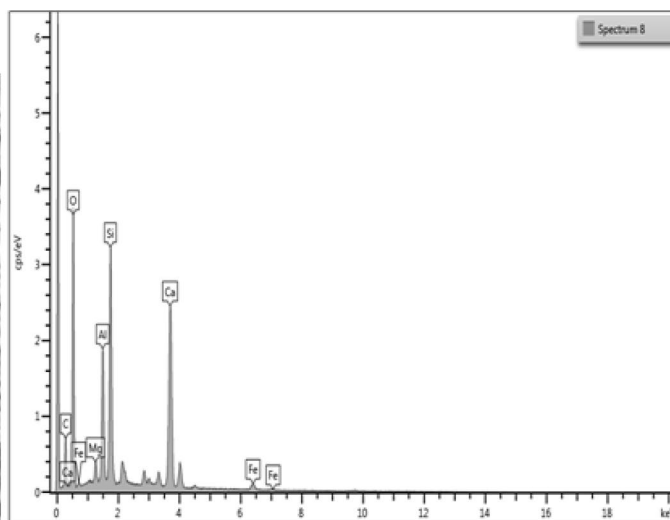
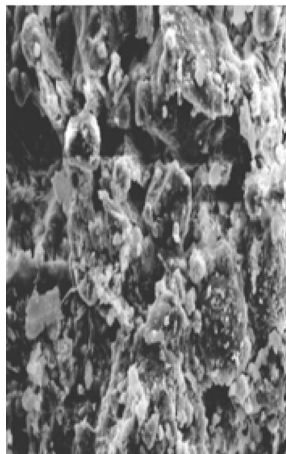


**Fig. 17** FM 0 reference concrete mix X-ray diffractogram (*A* anorthite, *Q* quartz)

mix revealed calcium, silica, alumina, oxygen, iron oxide, magnesium, and potassium peaks.

### X-ray diffraction

X-ray diffraction analysis of reference concrete mix and FA-based prepared mixes is illustrated in Figs. 17, 18, 19, and 20. Figure 17 depicts the XRD pattern of a reference mix (FM0), with quartz (silica oxides) and anorthite forming the major peaks. Figure 18 demonstrates XRD peaks of portlandite (calcium hydroxide) and quartz formed in a fly ash-prepared mixture (FM10) containing 10% fly ash as supplementary cementitious materials. Figure 19 demonstrates that the peaks of anorthite, portlandite, calcite, and quartz were formed with 15% fly ash. The XRD peaks of portlandite, quartz, and calcite were formed when a concrete mixture contained 30% fly ash. Figures 17, 18, 19, and 20 demonstrate that the peaks of  $C_3S$ ,  $C_2S$ , and  $C_4AF$

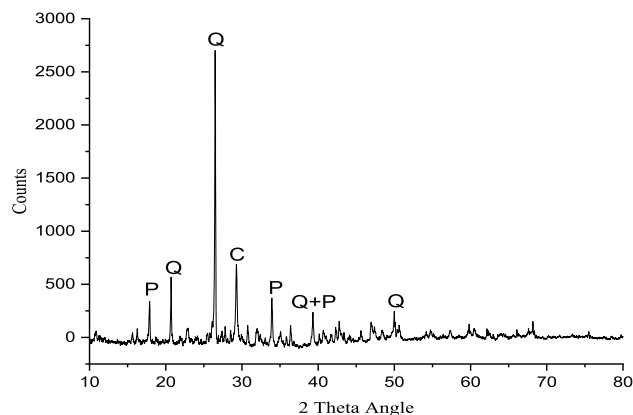


**Fig. 18** FM 10 concrete mix X-ray diffractogram (*P* portlandite, *Q* quartz, *C* calcite)

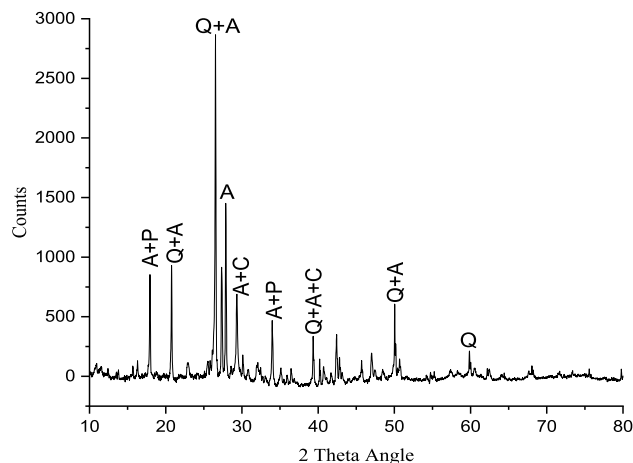


**Fig. 19** FM 15 concrete mix X-ray diffractogram (*A* anorthite, *P* portlandite, *Q* quartz, *C* calcite)

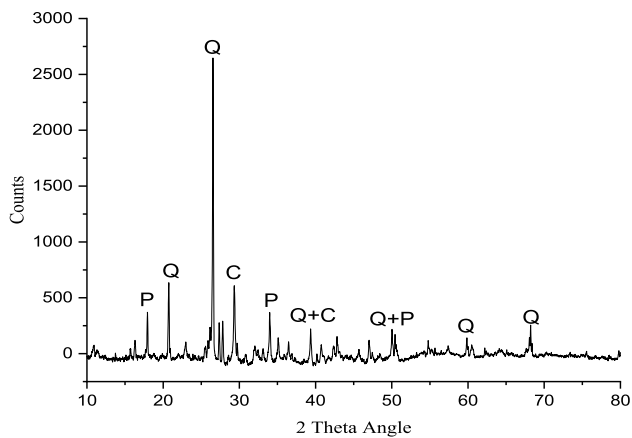


**Fig. 20** FM 30 concrete mix X-ray diffractogram (*P* portlandite, *Q* quartz, *C* calcite)

are not visible, inferring that these components have been completely consumed after 28 days.

**Effect of silica oxide ( $\text{SiO}_2$ )/quartz** The peak value or intensity of silica oxides in FM0 (reference concrete mixture) was 2600 obtained at 2 theta of 26.50 with  $d(A)=3.3612$ . The peak intensity of silica oxide or quartz for FM10 concrete mix is approximately 2700 with  $d(A)=3.3442$  obtained at 2 theta of 26.63, which is relatively close to the peak intensity of FM0 mix, which is 2600 at 26.50. This is due to the use of copper slag and fly ash in the FM10 mix versus reference mixes. Because of the increased amount of fly ash content in these mixtures, there was also a significant variation in peak intensities for FM10, FM15, and FM30 mixes. Peak intensity or value increases to around 2850 with  $d(A)=3.3439$  at 2 theta of 26.64 in FM15 mix and decreases to around 2550 with  $d(A)=3.3427$  at 26.65 in FM30 mix. Furthermore, the compressive strength of the FM10 mix is the highest of all fly ash replacement mixes (FM10, FM15, and FM30), indicating that silica has been used to its full potential for maximum C–S–H gel formation, resulting in enhanced cement-aggregate composite binding. Silica has a favorable effect on concrete strength generation since it reacts with the majority of calcium hydroxide that is formed during the hydration reaction within 28 days. It thus enhances concrete's strength in compression. The reaction of silica with  $\text{Ca}(\text{OH})_2$  developed across particles of sand, as well as with calcium hydroxide distributed all across the paste, affects the matrix's particle size distribution, which in significantly influences the concrete's compressive strength [36].

**Effect of portlandite (calcium hydroxide)** We can see in Fig. 14 that there were no peaks of portlandite in the reference mix; it is because of all calcium hydroxide convert

in secondary C–S–H gel by pozzolanic action. In the case of FM10 concrete mix, a higher peak value of 118.62 with  $d(A)=4.9149$  and 159.80 with  $d(A)=2.6297$  in counts/second at 2 theta of 18.63 and 34.07, respectively. It is greater than the FM15 concrete mix and FM30 mix. Overall, calcium hydroxide adds less to the strength and non-permeability of concrete because it fills voids or reduces pore volume by transforming liquid into solid or crystal manner. As a result, the FM10 mix (with a high  $\text{Ca}(\text{OH})_2$  peak value) has the most strength and the least permeability of all mixes. The only disadvantage of greater calcium hydroxide content is that it reduces concrete durability [34]. The number of peaks in the FM30 mix results in a lower concentration of  $\text{Ca}(\text{OH})_2$  crystals than in other mixtures, according to XRD analysis.

**Effect of calcite** The effectiveness of (calcite) calcium carbonate in fly ash-based prepared mixes is also demonstrated by the XRD technique when compared to the reference mix. Calcite peaks were 245.83 (FM10 mix) at 2 theta = 29.42. In the case of FM15, the peaks were 212.53 and 136.04 at 2 theta values of 29.41 and 39.45, respectively. FM30 mix also has a peak value of 231.46 at 29.43 2theta. There were no peaks seen in reference concrete mix XRD. Since the percentage of calcite is less compared to silica oxide and anorthite, calcite has little impact on the quality of concrete.

**Effect of anorthite** X-ray diffraction of the reference mix shows the anorthite having major peaks of 223.56, 189.23, 235.75, 314.64, and 110.63 at 2 theta angles of 17.89, 27.31, 29.27, 33.95, and 46.97, respectively. Reference concrete mix shows the predominance of anorthite peaks in reference to FA-based prepared mixes. The major XRD peaks of anorthite in FM15 concrete mix were 322.89 and 518.14 at 2 theta of 27.42 and 27.99, respectively.

## Conclusion

The study looked at how using fly ash (FA) and (CS + CBA) as partial replacements for cement and natural fine aggregate, respectively, affected the microstructural, hardened, and fresh properties of concrete mixtures. Test results revealed that the optimal quantity was 20% replacement, i.e., 20% FA as cement and (20% CS + 20% CBA) as sand. It gives greater strength with a higher percentage of replacement. Because of the spherical shape of fly ash and the low moisture absorption and gelatinous texture of copper slag, the use of FA, CS, and CBA improves the workability of the concrete mixture. In comparison with the reference mix, the compressive and split tensile strength improves with increasing percentage replacement up to 25%. At 10% replacement, the maximum compressive strength is obtained. Scanning

electron microscopic analysis reveals that dense C–S–H gel and very few ettringite needles were seen in 10% replacement concrete mix leading to strength increment. Also, the higher percentage of fly ash and coal bottom ash leads to a large number of voids and loosely packed structures in a 30% replacement mix, resulting in a decrease in compressive strength. Furthermore, X-ray diffraction analysis confirms that the best possible silica consumption has occurred for the greatest calcium silicate hydrate gel formation in 10 and 15% percentage replacement, resulting in enhanced cement-aggregate composite binding action and increased strength. The use of additives like fly ash gradually improves the workability of the concrete mix up to 25% on mixing it 0–30% with 5% intervals and changes in microstructural characteristics resulting in higher strength.

**Acknowledgements** This work was supported by the Madan Mohan Malaviya University of Technology, Gorakhpur.

**Funding** Nil.

## Declarations

**Conflict of interest** No conflict of interest.

## References

- Rana A, Kalla P, Csetenyi LJ (2015) Sustainable use of marble slurry in concrete. *J Clean Prod* 94:304–311
- Pathak PP (2009) Inclusion of Portland and pozzolana (fly ash waste) cement in specifications. *Ind Highw* 37(4):2
- Rafeizonooz M, Mirza J, Salim MR, Hussin MW, Khankhaje E (2016) Investigation of coal bottom ash and fly ash in concrete as replacement for sand and cement. *Constr Build Mater* 116:15–24
- Yang KH, Jung YB, Cho MS, Tae SH (2015) Effect of supplementary cementitious materials on reduction of CO<sub>2</sub> emissions from concrete. *J Clean Prod* 103:774–783
- Nie S, Zhou J, Yang F, Lan M, Li J, Zhang Z, Sanjayan JG (2022) Analysis of theoretical carbon dioxide emissions from cement production: methodology and application. *J Clean Prod* 334:130270
- IBEF, India Brand Equity Foundation. [www.ibef.org/industry/cement-india.aspx](http://www.ibef.org/industry/cement-india.aspx), 2022 (accessed 09.09.22)
- Mardani-Aghabaglou A, Tuyan M, Ramyar K (2015) Mechanical and durability performance of concrete incorporating fine recycled concrete and glass aggregates. *Mater Struct* 48(8):2629–2640
- Khankhaje E, Hussin MW, Mirza J, Rafeizonooz M, Salim MR, Siong HC, Warid MNM (2016) On blended cement and geopolymer concretes containing palm oil fuel ash. *Mater Des* 89:385–398
- Ashish DK (2018) Feasibility of waste marble powder in concrete as partial substitution of cement and sand amalgam for sustainable growth. *J Build Eng* 15:236–242
- Ozkan O, Yuksel I, Muratoglu O (2007) Strength properties of concrete incorporating coal bottom ash and granulated blast furnace slag. *Waste Manage* 27(2):161–167
- Aggarwal Y, Siddique R (2014) Microstructure and properties of concrete using bottom ash and waste foundry sand as partial replacement of fine aggregates. *Constr Build Mater* 54:210–223
- Singh M, Siddique R (2014) Strength properties and micro-structural properties of concrete containing coal bottom ash as partial replacement of fine aggregate. *Constr Build Mater* 50:246–256
- Fly ash management: legal requirement and other issues, presentation by Ms. Sanchita Jindal, MoEF
- Singh M, Siddique R (2013) Effect of coal bottom ash as partial replacement of sand on properties of concrete. *Resour Conserv Recycl* 72:20–32
- Zhou H, Bhattarai R, Li Y, Si B, Dong X, Wang T, Yao Z (2022) Towards sustainable coal industry: turning coal bottom ash into wealth. *Sci Total Environ* 804:149985
- Sharma R, Khan RA (2017) Durability assessment of self compacting concrete incorporating copper slag as fine aggregates. *Constr Build Mater* 155:617–629
- ICSG (2021) ICSG Releases Latest Copper Market Forecast 2021–2022. Available from: <http://www.icsg.org/index.php/111-icsg-releases-latest-copper-market-forecast-2021-2022>
- Sharma R, Khan RA (2017) Sustainable use of copper slag in self compacting concrete containing supplementary cementitious materials. *J Clean Prod* 151:179–192
- Shi C, Meyer C, Behnood A (2008) Utilization of copper slag in cement and concrete. *Resour Conserv Recycl* 52:1115–1120
- Obe RKD, de Brito J, Mangabhai R, Lye CQ (2016) Sustainable construction materials: copper slag. Woodhead Publishing
- Gorai B, Jana RK (2003) Characteristics and utilisation of copper slag—a review. *Resour Conserv Recycl* 39(4):299–313
- Supekar N (2007) Utilisation of copper slag for cement manufacture construction management and review. Sterlite Industries (I) Ltd, Tuticorin
- Prem PR, Verma M, Ambily PS (2018) Sustainable cleaner production of concrete with high volume copper slag. *J Clean Prod* 193:43–58
- Yüksel İ, Bilir T, Özkan Ö (2007) Durability of concrete incorporating non-ground blast furnace slag and bottom ash as fine aggregate. *Build Environ* 42(7):2651–2659
- Bilir T (2012) Effects of non-ground slag and bottom ash as fine aggregate on concrete permeability properties. *Constr Build Mater* 26(1):730–734
- Singh G, Chaurasia S (2022) Feasibility of waste copper slag with coal bottom ash in concrete as partial substitution of fine aggregate. *Innov Infrastruct Solut* 7(2):1–13
- Rathe M, Singh N (2022) Durability properties of copper slag and coal bottom ash based I-shaped geopolymer paver blocks. *Constr Build Mater* 347:128461
- IS: 1489–1991 (Part-I). Portland Pozzolana cement specification. New Delhi, India: Bureau of Indian Standard
- IS383 (2016) Coarse and Fine Aggregates from Natural Sources for Concrete—Specification. Bureau of Indian Standards, pp. 1–29. ICS No. 91.100.30 (CED 2-7992)
- Saeed KR (1995) Technique of multi-step concrete mixing. *Mater Struct* 28(4):230–234
- BIS: 516-1959. Indian standard code of practice- methods of test for strength of concrete, Bureau of Indian Standards, New Delhi, India
- BIS: 5816-1999 (1999) Indian standard splitting tensile strength of concrete-test method. New Delhi, India: Bureau of Indian Standards.
- Ranjbar N, Mehrali M, Behnia A, Alengaram UJ, Jumaat MZ (2014) Compressive strength and microstructural analysis of fly ash/palm oil fuel ash based geopolymer mortar. *Mater Des* 59:532–539
- Sata V, Jaturapitakkul C, Kiattikomol K (2007) Influence of pozzolan from various by-product materials on mechanical properties of high-strength concrete. *Constr Build Mater* 21(7):1589–1598
- Kou SC, Poon CS, Chan D (2007) Influence of fly ash as cement replacement on the properties of recycled aggregate concrete. *J Mater Civ Eng* 19(9):709–717



36. Singh S, Khan S, Khandelwal R, Chugh A, Nagar R (2016) Performance of sustainable concrete containing granite cutting waste. *J Clean Prod* 119:86–98

author(s) or other rightsholder(s); author self-archiving of the accepted manuscript version of this article is solely governed by the terms of such publishing agreement and applicable law.

Springer Nature or its licensor (e.g. a society or other partner) holds exclusive rights to this article under a publishing agreement with the